First-principles study of the elastic properties of In-Tl random alloys

Chun-Mei Li,[1,2,][*] Qing-Miao Hu,[2,1] Rui Yang,[2] Börje Johansson,[1,3] and Levente Vitos[1,3,4]

[1]*Applied Materials Physics, Department of Materials Science and Engineering,*
Royal Institute of Technology, Stockholm SE-100 44, Sweden
[2]*Shenyang National Laboratory for Materials Science, Institute of Metal Research,*
Chinese Academy of Sciences, 72 Wenhua Road, Shenyang 110016, China
[3]*Condensed Matter Theory Group, Physics Department, Uppsala University, Uppsala SE-75121, Sweden*
[4]*Research Institute for Solid State Physics and Optics, P.O. Box 49, Budapest H-1525, Hungary*

The composition-dependent lattice parameters and elastic constants of $In_{1-x}Tl_x (0 < x \leq 0.4)$ alloy in face-centered-cubic (fcc) and face-centered-tetragonal (fct) crystallographic phases are calculated by using the first-principles exact muffin-tin orbitals method in combination with coherent-potential approximation. The calculated lattice parameters and elastic constants agree well with the available theoretical and experimental data. For pure In, the fcc phase is mechanically unstable as shown by its negative tetragonal shear modulus C'. With Tl addition, C' of the fcc phase increases whereas that of the fct phase decreases, indicating that the fcc phase becomes mechanically more stable and the fct phase becomes less stable. In addition, the structural energy difference between the fcc and fct phases decreases with x. Both of these effects account for the observed lowering of the fcc-fct martensitic transition temperature upon Tl addition to In. The density of states indicates that the stability of the fct phase relative to the fcc one at low temperatures is due to the particular electronic structure of In and In-Tl alloys.

I. INTRODUCTION

Indium-thallium alloys in the composition range of $16-31$ at. % Tl undergo a martensitic transition from the high-temperature face-centered-cubic (fcc) phase to the low-temperature face-centered-tetragonal (fct) phase.[1,2] This transition is of particular interests since it exhibits distinct first-order transition but nearly second order.[1,3]

The knowledge of the elastic constants in general is crucial for understanding the structural transformation. The martensitic transformation (MT) in In-Tl is accompanied by a pronounced softening of the shear modulus $C' = \frac{1}{2}(C_{11} - C_{12})$. This unusual softening behavior was proposed resulting from the combination of reversible twinning and changes in the unit cell on a very fine scale in the alloy.[4] Efforts have been made to measure the elastic moduli of several In-Tl alloys in either fct or fcc structures.[4–6] According to the experiments by Gunton and Saunders,[5] at room temperature, C' decreases from 2.7 GPa (corresponding to pure In) to 1.8 GPa (1.2 GPa) when 12 at. % (15 at. %) Tl is added to body-centered tetragonal (bct) In. On the other hand, C' of fcc In-Tl with $24-27$ at. % Tl approaches zero.[4,5] Despite numerous experimental investigations, a systematic study of the elastic parameters of In-Tl alloy in different lattice structures is still demanded in order to understand the composition-dependent phase transition.

Nowadays, first-principles methods based on density-functional theory[7,8] are employed routinely to evaluate the elastic constants of materials. Yang *et al.*[9] and Do *et al.*[10] have calculated the elastic constants of pure In using tight-binding (TB) and plane-wave pseudopotential (PWPP) methods, respectively. The TB calculations by Yang *et al.*[9] generated C_{44} and C_{66} almost twice the experimental values.[11–13] The elastic constants from the PWPP calculation by Do *et al.*[10] are in a good agreement with the experimental measurements. Unfortunately, due to the inconvenience of the first-principles method in treating random alloy, the first-principles investigation of the elastic properties of In-Tl alloy has not yet been addressed. Recent implementation of the exact muffin-tin orbital (EMTO) (Refs. [14–18]) theory in combination with the coherent-potential approximation (CPA) (Refs. [19] and [20]) describes reliably the elastic parameters of various random alloys such as Fe-Cr, Ag-Zn, etc.[18,21–27] Adopting the EMTO-CPA method, here we investigate systematically the composition-dependent elastic properties of In-Tl alloy in both cubic and tetragonal structures.

The rest of the paper is arranged as follows: in Sec. II, we describe the theoretical methods employed in the present work, i.e., *ab initio* EMTO-CPA method. In Sec. III, the composition-dependent lattice parameters and elastic constants of $In_{1-x}Tl_x$ ($0 \leq x \leq 0.4$) alloys are presented. The relative stability of the fcc and fct phases is discussed using the calculated elastic constants, the total-energy difference, and the electronic density of states (DOS). Finally, we summarize our main results in Sec. IV, and in the Appendix, we briefly review the technique used to calculate the elastic constants of cubic and tetragonal crystals.

II. METHODS AND CALCULATIONS DETAILS

All calculations were performed by using the first-principles EMTO method.[14–18] EMTO is an improved screened Koringa-Kohn-Rostoker method. In contrast to the usual muffin-tin-based methods, within EMTO theory, the one-electron states are determined exactly (within the common numerical errors, such as the one cutoff, numerical integrations, etc.) for an optimized overlapping muffin-tin potential. This potential is chosen as the best possible spherical

TABLE I. Theoretical (present results obtained using the LDA, PBE, and AM05 approximations) equilibrium lattice parameters (in Å), bulk modulus (in GPa) of pure fct and fcc In and hcp Tl, and the total-energy difference ΔE (in mRy/atom) between fcc and fct In ($\Delta E = E^{\text{fcc}} - E^{\text{fct}}$). For comparison the available theoretical results and experimental data are also included. PAW stands for projector augmented wave and PW91 is the exchange-correlation approximation by Perdew and Wang (Ref. 33).

Phase	Method	a	c	c/a	B	ΔE
fct-In	LDA	4.438	5.068	1.142	47.7	
	PBE	4.612	5.220	1.132	32.8	
	AM05	4.595	5.289	1.151	41.1	
	Expt.[a]	4.600	4.947	1.076	41.1	
	PAW-LDA[b]	4.473	4.923	1.101	50.6	
	PAW-PW91[b]	4.677	5.030	1.076	35.8	
	TB[c]	4.204	4.815	1.146	52.0	
fcc-In	LDA	4.646			46.4	+0.70
	PBE	4.825			32.5	+0.37
	AM05	4.706			40.7	+0.60
	Expt.[d]					+0.07
	PAW-LDA[b]	4.620			49.1	+0.19
	PAW-PW91[b]	4.792			35.7	+0.06
	TB[c]	4.651			52.0	+3.68
hcp-Tl	LDA	3.254	5.210	1.601	41.6	
	PBE	3.421	5.416	1.583	31.0	
	AM05	3.325	5.310	1.597	31.5	
	Expt.[e]	3.463	5.539	1.599	34.0	

[a]Reference 34.
[b]Reference 10.
[c]Reference 9.
[d]Reference 35.
[e]Reference 36.

approximation to the exact potential, compared to the conventional muffin-tin or nonoverlapping approach.[15,18,28] The radii of the potential spheres, the spherical potential waves, and the constant potential in the interstitial region are calculated by minimizing the deviation between the exact and overlapping potentials and the errors coming from the overlap between spheres. With these improvements and with the full charge-density technique for the total energy,[29] the EMTO method is suitable to describe accurately the total energy with respect to anisotropic lattice distortions. Another advantage of the EMTO method compared to other first-principles methods such as plane-wave methods is that, the CPA (Refs. 19 and 20) can be conveniently incorporated. This greatly facilitates the calculations of the systems with chemical disorder at first-principles level. The accuracy of the EMTO-CPA method for the equation of state and elastic properties of metals and disordered alloys has been demonstrated in a number of former works.[17,18,21–27]

In the present application, the EMTO basis sets included s, p, d, and f components. The Green's function was calculated for 32 complex energy points distributed exponentially on a semicircular contour. For the muffin-tin potential sphere (R_{mt}), the usual setup $R_{mt} = R_{ws}$, with R_{ws} being the Wegner-Seitz radius, was selected. In the one-center expansion of the full charge density, the number of components was truncated at 8, and the scalar-relativistic and soft-core approximations

were adopted. The In $4d^{10}5s^24p^1$ and Tl $5d^{10}6s^26p^1$ states were treated as the valence states. The exchange-correlation term was described using the AM05 functional developed by Armiento and Mattsson.[30] For fcc and fct In and hexagonal-close-packed (hcp) Tl, the ground-state properties obtained using the local-density approximation (LDA) (Ref. 31) and generalized gradient approximation by Perdew, Burke, and Ernzerhof (PBE) (Ref. 32) are also presented. Throughout of our calculations, the Brillouin zone was sampled by a 17 $\times 17 \times 17$ uniform k-point mesh without any smearing technique. The error bars for the elastic constants are estimated from the accuracy of the numerical fit for the energy change versus distortion.

III. RESULTS AND DISCUSSION

A. Elastic constants of pure In

Table I lists the equilibrium lattice parameter, bulk modulus of pure fct and fcc In and hcp Tl, and the total-energy difference between fcc and fct In, in comparison with the other theoretical and experimental values. As expected, LDA underestimates the lattice parameters and overestimates the bulk modulus for both fct and fcc In and hcp Tl. For fct In, PBE generates c/a (1.132) in better agreement with the experimental value (1.076) than AM05 (1.151). The AM05 c/a

TABLE II. Theoretical elastic constants (in GPa) and Debye temperature (Θ, in K) for pure fct and fcc In, respectively, in comparison with the available theoretical results and experimental data. The estimated theoretical error bars are also shown.

Phase	Method	C_{11}	C_{12}	C_{13}	C_{33}	C_{44}	C_{66}	C'	Θ
fct	LDA	57.8 ± 1.57	44.2 ± 1.57	42.9 ± 0.92	53.6 ± 3.70	11.2 ± 0.19	25.1 ± 0.48	6.8 ± 1.30	136.5
	PBE	38.1 ± 1.96	28.3 ± 1.96	30.7 ± 0.76	39.6 ± 2.10	7.2 ± 0.07	14.9 ± 0.36	4.9 ± 1.12	111.1
	AM05	49.1 ± 1.84	37.3 ± 1.84	38.8 ± 0.45	46.6 ± 2.67	6.6 ± 0.06	15.7 ± 0.42	5.9 ± 0.99	113.1
	Expt. (298 K)[a]	44.4	39.4	40.4	44.3	6.5	12.2	2.5	
	Expt. (300 K)[b]	45.4	40.1	41.5	45.2	6.5	12.1	2.7	
	Expt. (77 K)[b]	52.6	40.6	44.6	50.8	7.6	16.0	6.0	
	Expt. (4.2 K)[b]	53.9	38.7	45.1	51.6	8.0	16.8	7.6	
	Expt. (0 K)[b]								111.3
	PAW-LDA	69.6	36.2	46.2	57.5	13.7	17.6	16.7	
	PAW-PW91[c]	44.6	25.8	33.9	41.4	5.6	13.3	9.4	
	TB[d]					13.4	22.6	4.2	
fcc	LDA	40.9 ± 2.09	49.1 ± 1.05			14.9 ± 0.54		-4.1 ± 1.57	
	PBE	30.6 ± 1.05	33.4 ± 0.53			11.7 ± 0.11		-1.4 ± 0.79	
	AM05	35.9 ± 1.99	43.1 ± 0.99			13.0 ± 0.48		-3.6 ± 1.49	
	PAW-LDA[c]	42.4	52.5			10.2		-5.1	
	PAW-PW91[c]	35.1	36.0			5.5		-0.5	

[a]Reference 12.
[b]Reference 13.
[c]Reference 10.
[d]Reference 9.

ratio, on the other hand, is in agreement with that from TB calculation (1.146) (Ref. 9) but slightly larger than those from the experiment[34] and the first-principles projected augmented wave (PAW) calculations.[10] This discrepancy may partly be ascribed to the muffin-tin approximation employed in the present study. We note that the actual equilibrium c/a sensitively depends on the potential sphere radii. For instance, when setting the muffin-tin potential sphere to $R_{mt} = 1.05 R_{ws}$, the equilibrium c/a ratio of the fct In turns out to be about 1.090. It is noted that for all the theoretical calculations, the fcc In is higher in energy than the fct one which explains the stable fct structure of In at lower temperature. For hcp Tl, PBE yields lattice parameters a and c in better agreement with the experimental values[36] than LDA and AM05. However, the theoretical c/a from all three functionals are close to each other, and in good agreement with experimental measurement.[36]

Table II presents the calculated elastic constants and Debye temperature (Θ) of the fct and fcc In in comparison with those from other theoretical calculations and experimental measurements. For both fct and fcc phases, the elastic constants from AM05 are in between those from LDA and PBE. PBE underestimates most of the elastic constants except C_{44} and C_{66} whereas LDA overestimates seriously C_{66}. In general, AM05 elastic constants are in better agreement with those from experimental measurements at low temperature (77 K) than those corresponding to the LDA and PBE approximations. The largest error is only about 14% for C_{13}. The AM05 elastic Debye temperature (Θ) for a polycrystalline In is about 113.1 K, which is very close to the experimental value of 111.3 K.[13] Because of these, for the alloys we will present results obtained using this approximation only.

For fcc In, we get negative C' from the three approximations since C_{11} is smaller than C_{12}, which is in line with the first-principles PAW calculations.[10] The dynamical or mechanical stability condition of a lattice implies that the energy change $\Delta E \sim V C_{ij} e_i e_j$ upon any small deformation is positive. This condition can be formulated in terms of elastic constants. The stability criteria for cubic crystals requires that $C_{11} > |C_{12}|$, $C_{11} + 2C_{12} > 0$, and $C_{44} > 0$, and for tetragonal crystals is that $C_{11} > |C_{12}|$, $C_{33} > 0$, $C_{44} > 0$, $C_{66} > 0$, $(C_{11} + C_{33} - 2C_{13}) > 0$, and $(2C_{11} + C_{33} + 2C_{12} + 4C_{13}) > 0$. From our calculations, the theoretical elastic constants of fct In satisfy all of the conditions, whereas those of fcc In do not meet the condition $C_{11} > |C_{12}|$ since C' is minus. Therefore, at 0 K, fcc In is not thermodynamically stable and the pure In is stabilized by fct structure.

B. Lattice parameters of In-Tl alloys

In order to investigate the composition dependence of elastic properties of $In_{1-x}Tl_x$ ($0 \le x \le 0.4$) random alloys, first we calculate the equilibrium lattice parameters for both fct and fcc phases as a function of the composition of the alloy. Figure 1 displays the equilibrium a and c/a ratio of the fct phase, in comparison with those from experimental measurements.[1,42] It is seen that with increasing x, a increases whereas c/a ratio decrease almost linearly. The trends of both a and c/a ratio are in accordance with the experimental measurement. The calculated a values are in perfect agreement with the experimental data whereas the theoretical c/a ratios are slightly larger than those from experiments.
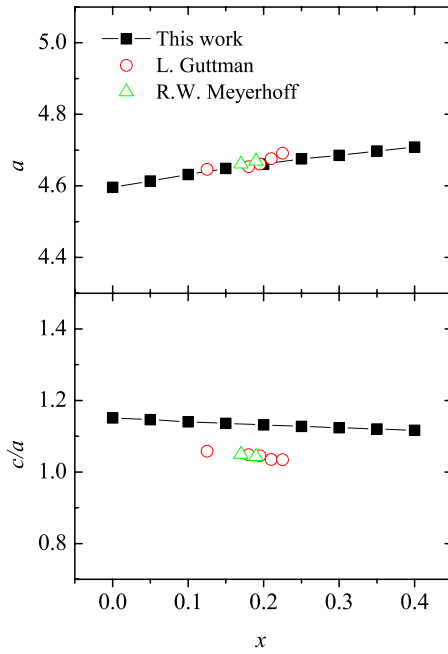
FIG. 1. (Color online) Lattice parameters (a in angstrom and c/a) of fct $In_{1-x}Tl_x$ ($0 \leq x \leq 0.4$) alloys as a function of x. The experimental data are from Refs. 1 and 42.

The c/a ratio of the tetragonal phase has been related to the martensitic transition temperature T_M of the alloys such as Ni_2MnGa alloy undergoing the cubic to tetragonal phase transition with lowering temperature.[37,38] According to this correlation, a larger $|c/a-1|$ corresponds to a higher T_M. From our calculations, the $|c/a-1|$ ratio of $In_{1-x}Tl_x$ alloys decreases with increasing x, indicating that T_M should decrease accordingly. This is in line with the experiments showing that T_M of $In_{1-x}Tl_x$ decreases from about 400 to 0 K with x increasing from about 0.2 to 0.3.[39–41]

Figure 2 shows the composition-dependent lattice parameter a of the fcc $In_{1-x}Tl_x$. As seen from the figure, a increases almost linearly with increasing x. For $x > 0.2$, the calculated a values are in perfect agreement with those from experiments.[1,42] The experimental a of fcc $In_{1-x}Tl_x$ with $x < \sim 0.2$ is not available since in this composition range the fcc phase is not stable.
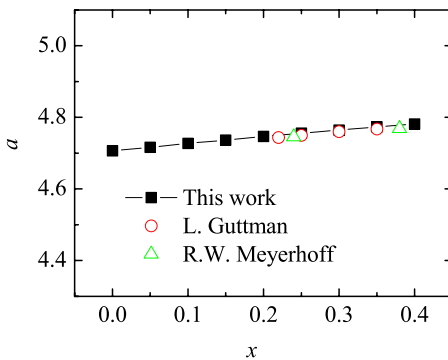
FIG. 2. (Color online) Lattice parameter (a in Å) of fcc $In_{1-x}Tl_x$ ($0 \leq x \leq 0.4$) alloys as a function of x. The experimental data are from Refs. 1 and 42.
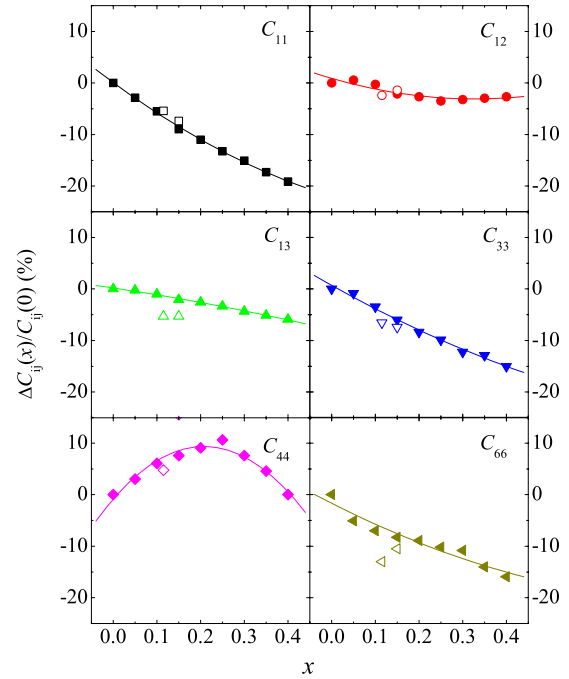
FIG. 3. (Color online) The relative change in the elastic constants of fct $In_{1-x}Tl_x$ ($0 \leq x \leq 0.4$) alloys as a function of x. The experimental results are from Ref. 5.

C. Elastic constants of In-Tl alloys

Using the equilibrium lattice structures determined in Sec. III B, we calculated the elastic constants of $In_{1-x}Tl_x$ alloys. Figures 3 and 4 show the elastic constants relative to those of the pure In for both fct and fcc phases, as function of x. As shown in Fig. 3, for the tetragonal phase, C_{11}, C_{33}, and C_{66} decrease significantly with increasing x: for $x=0.4$, C_{11} is
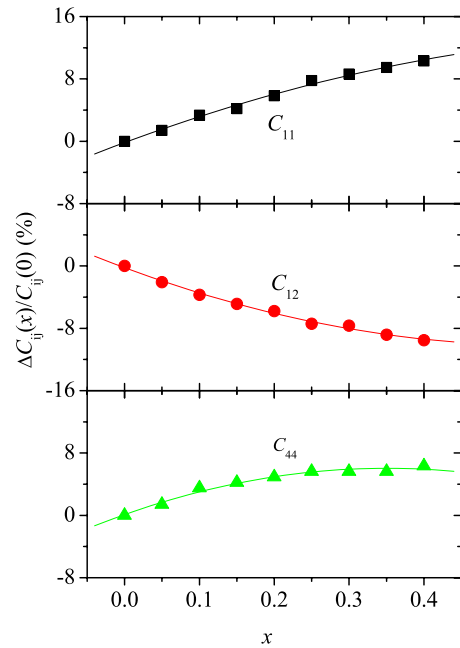
FIG. 4. (Color online) The relative change in the elastic constants of fcc $In_{1-x}Tl_x$ ($0 \leq x \leq 0.4$) alloys with the composition x.
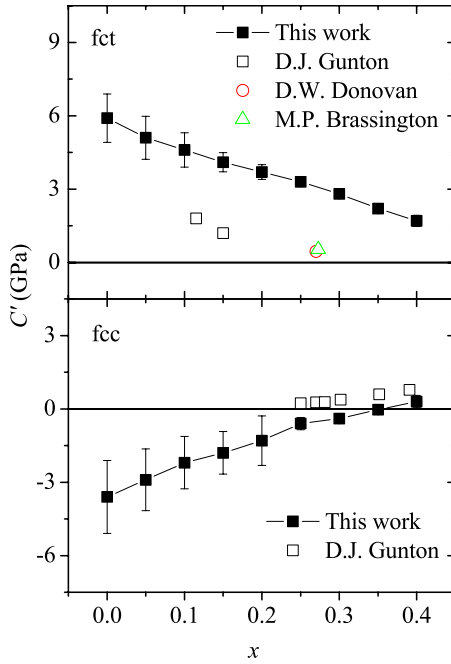
FIG. 5. (Color online) The composition dependence of shear modulus C' of $In_{1-x}Tl_x$ ($0 \le x \le 0.4$) alloys with fct (upper panel) and fcc (lower panel) structures. The experimental data are from Refs. 5, 50, and 51.

20% smaller than that of pure In whereas C_{33} and C_{66} reduce about 15%. C_{13} also decreases linearly with increasing x but the decreasing is moderate compared to C_{11}, C_{33}, and C_{66}: with x up to 0.4, C_{13} decreases about 5%. The variation in C_{12} and C_{44} with x is quite small and nonlinear. C_{12} decreases slightly with increasing x and remains almost constant with $x > \sim 0.25$. C_{44} increases slightly with x up to $x = 0.25$ and then decreases with increasing x for $x > \sim 0.25$.

Figure 4 shows the variation in the elastic constants of fcc $In_{1-x}Tl_x$ against x. It is seen that C_{11} increases whereas C_{12} decreases with increasing x. C_{44} first increases with x and then remains almost unchanged for $x > \sim 0.25$.

The MT of In-Tl alloys results from the soft-phonon modes and their accompanying soft tetragonal shear modulus $C' = \frac{1}{2}(C_{11} - C_{12})$ of the high-temperature fcc phase.[6,43] For alloys undergoing MT, the composition dependence of T_M is generally related to the composition dependence of C': the lower the elastic constant the higher the T_M will be.[44–46] This relationship is confirmed for both TiNi-based shape memory alloys and various kinds of off-stoichiometric Ni_2MnGa alloys.[47–49] In order to correlate the elastic stability with the MT, we calculated the tetragonal shear moduli C' of both fct and fcc $In_{1-x}Tl_x$ alloys as shown in Fig. 5. C' of the fct phase is larger whereas C' of the fcc phase is slightly smaller than the experimental value. The reason is that our elastic constants are calculated at 0 K but the experimental values were measured at finite temperature. A typical feature of the In-Tl alloys is that C' of the fct martensitic phase decreases and that of the fcc austenite increases with increasing temperature,[4,13] such as shown in Table II, for pure In in fct phase, $C' = 7.6$ GPa at 4.2 K, whereas around room temperature (298 K), C' turns out to be 2.5 GPa, only about one third of that value corresponding to 4.2 K.
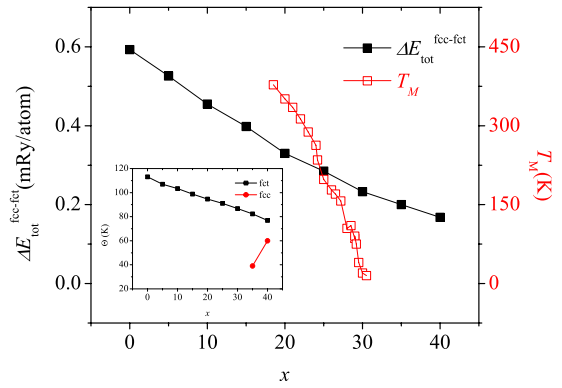
FIG. 6. (Color online) The total-energy difference $\Delta E_{tot}^{fcc-fct}$ between fcc and fct phases and the Debye temperature Θ in both fct and fcc $In_{1-x}Tl_x$ alloy (in the inset) with respect to x ($0 \le x \le 0.4$). Presented also in the figure is the experimental martensitic transition temperature T_M from Refs. 39–41.

The present calculations reproduce well the experimental trends of C' against the compositions for both phases: C' of fct decrease and C' of the fcc phase increases with increasing x. The fcc phase becomes mechanically stable for $x > \sim 0.30$, where C' becomes positive. These trends indicate that the low-temperature fct phase becomes mechanically soft (less stable) whereas the high-temperature fcc phase becomes more stable, corresponding to lowering MT temperature. This is in accordance with experimental measurements of the MT temperature showing that the MT temperature decreases from about 400 to 0 K with x increasing from about 0.2 to 0.3.[39–41]

D. Phase stability

The relative phase stability can be measured by the total-energy difference between the two competing phases: $\Delta E_{tot}^{fcc-fct} = E^{fcc} - E^{fct}$ with E^{fcc} and E^{fct} being the energies of the fcc and fct phases, respectively. Figure 6 shows $\Delta E_{tot}^{fcc-fct}$ as a function of the concentration of Tl together with the experimental martensitic transition temperature (right axis). It is seen that, with increasing x, $\Delta E_{tot}^{fcc-fct}$ decreases, indicating the fct phase becomes thermodynamically less stable relative to the fcc phase. This results in lowering martensitic transition temperature, in agreement with the experimental finding. We should also note that the $\Delta E_{tot}^{fcc-fct} > 0$ for all compositions considered here, meaning that at static conditions (without any phonon contribution) the fct structure remains the stable phase.

Due to the softer C' of the fcc phase than that of the fct phase, the fcc phase can be further stabilized by the lattice vibration effect. At 0 K, the zero-point vibrational energy difference is approximately $\Delta F_{vib}^{fcc-fct} \approx \frac{9}{8} k_B \Delta \Theta$, where $\Delta \Theta$ is the difference of Debye temperatures between the fcc and fct phases, and k_B the Boltzmann constant. For $x = 0.35$, the Debye temperature evaluated from the calculated elastic constants is about 82.3 K for the fct phase and 39.0 K for the fcc phase as shown in the inset of Fig. 6. These yield a vibration energy difference of $\Delta F_{vib}^{fcc-fct} = -0.31$ mRy/atom. Thus, the overall free-energy difference $\Delta F_{tot}^{fcc-fct} = \Delta E_{tot}^{fcc-fct} + \Delta F_{vib}^{fcc-fct}$ re-
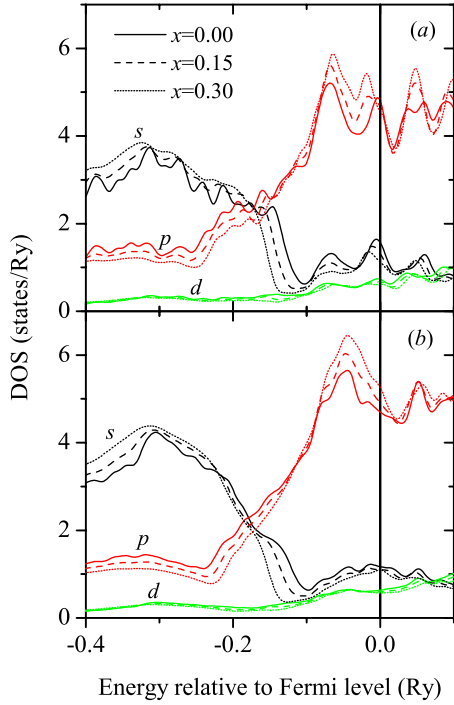
FIG. 7. (Color online) The DOS of In$_{1-x}$Tl$_x$ (x=0, 0.15, and 0.30) alloys for fcc (*a*) and fct (*b*) crystallographic phases. *s*, *p*, and *d* denote the three decomposed states of the total DOS. The vertical line indicates the Fermi level.

duces from +20 mRy/atom (corresponding to static conditions) to −0.11 mRy/atom. Therefore, the fcc In$_{1-x}$Tl$_x$ with x=0.35 turns out to be thermodynamically stable at 0 K, in perfect agreement with experimental finding. It is interesting to point out that the structural transition is realized by the phonon terms. Taking into account the present theoretical error bars for C' (Table II), from Fig. 5 we can see that the above transition might in fact occur already around 25−30 % Tl.

E. Electronic structure

In order to investigate the electronic origin of the composition dependence of phase stability of In-Tl binary alloy, we calculate the DOS for pure In and In$_{1-x}$Tl$_x$ (x=0.15 and x=0.30) alloys. The components of s, p, and d states of the total DOS are shown in Fig. 7. The DOS around the Fermi level is mainly governed by the p states of In/Tl with a small contribution from the s state. For the fcc phase of pure In (x=0), there exits a strong peak right at the Fermi level, which is ascribed to the degenerated nonbonding p states of the In atoms. The degenerated states split in the fct phase (Peierls distortion). Therefore, the Fermi level of fct In locates in a wide pseudogap from −0.05 to 0.05 Ry, indicating further hybridization between the p states of fct In atoms and stronger bonding between the In atoms than those in fcc phase. This is why the fct phase is more stable than the fcc phase of pure In at 0 K.

With increasing x, the number of p states at the Fermi level of the fcc phase remains almost unchanged. For the fct phase, however, the pseudogap becomes narrower, indicating weaker hybridization between the electronic orbitals. On the other hand, the Fermi level shifts away from the bottom of the pseudogap and the DOS at the Fermi level increases. Therefore, the fct phase becomes less stable (the kinetic energy increases). We conclude that the trend of DOS against the composition of the In$_{1-x}$Tl$_x$ alloy explains satisfactorily the decreasing stability of fct phase relative to that of the fcc one, in accordance with the calculated total-energy difference between these phases as shown previously in Fig. 6.

IV. CONCLUSION

Using the first-principles EMTO-CPA method, we have investigated the composition-dependent lattice parameters and elastic properties of In$_{1-x}$Tl$_x$ ($0 \leq x \leq 0.4$) random alloys in fcc and fct structures. With increasing x, both the fcc and fct lattice parameter a increases and the tetragonal c/a ratio decreases. Pure fcc-In is mechanically unstable (possesses negative tetragonal shear modulus C'). With increasing x, C' of the fcc phase increases and that of the fct phase decreases, indicating increasing stability of the fcc phase and decreasing stability of the fct phase and, therefore, lowering critical temperature of the fcc-fct martensitic transition temperature. The instability of the fcc phase at low temperatures is due to degenerated states near the Fermi level. These states split in the fct phase which stabilizes the fct phase. With increasing x, the fct phase becomes less stable (thermodynamically) because an alloying induced peak develops in the fct DOS near the Fermi level.

APPENDIX

At a fixed volume V, the elastic constants of a single crystal can be evaluated by straining the lattice and calculating the variation in the total energy induced by the strain. Applying a volume conserving strain tensor

$$\mathcal{D}(e) = \begin{pmatrix} 1+e_1 & \frac{1}{2}e_6 & \frac{1}{2}e_5 \\ \frac{1}{2}e_6 & 1+e_2 & \frac{1}{2}e_4 \\ \frac{1}{2}e_5 & \frac{1}{2}e_4 & 1+e_3 \end{pmatrix} \quad \text{(A1)}$$

to a crystal lattice, the total energy of the strained crystal can be written as

$$\Delta E(e_1, e_2, \ldots, e_6) = \frac{1}{2} V \sum_{i,j=1,6} C_{ij} e_i e_j + \mathcal{O}(e^3). \quad \text{(A2)}$$

With properly selected strain tensor, the elastic constants can be conveniently evaluated by fitting the $\Delta E(e_1, e_2, \ldots, e_6)$ as functions of e_i. In the above equation, we adopt the Voigt notation (xx, yy, zz, yz, xz, and xy are replaced by 1, 2, 3, 4, 5, and 6, respectively).

For a cubic crystal, $C_{11} = C_{22} = C_{33}$, $C_{12} = C_{13} = C_{23}$, and $C_{44} = C_{55} = C_{66}$. Therefore, three different deformations are needed to calculate the three independent elastic constants. In the present work, we first determine the bulk modulus B by fitting the calculated total energies versus volume (nine data points) to a Morse function,[52] from which we get the equilibrium volume as well. B is related to C_{11} and C_{12} as $B = \frac{1}{3}(C_{11} + 2C_{12})$. Then the shear moduli $C' = (C_{11} - C_{12})/2$ and C_{44} are calculated by using the volume conserving orthorhombic and monoclinic deformations, namely,

$$\begin{pmatrix} 1+\delta & 0 & 0 \\ 0 & 1-\delta & 0 \\ 0 & 0 & \dfrac{1}{1-\delta^2} \end{pmatrix}, \quad \text{(A3)}$$

which yields the energy change in $\Delta E(\delta) = 2VC'\delta^2 + \mathcal{O}(\delta^4)$, and

$$\begin{pmatrix} 1 & \delta & 0 \\ \delta & 1 & 0 \\ 0 & 0 & \dfrac{1}{1-\delta^2} \end{pmatrix}, \quad \text{(A4)}$$

which results in the energy change in $\Delta E(\delta) = 2VC_{44}\delta^2 + \mathcal{O}(\delta^4)$. C_{11} and C_{12} is then derived from $B = \frac{1}{3}(C_{11} + 2C_{12})$ and the shear modulus C'.

For a tetragonal crystal, $C_{11} = C_{22}$, $C_{13} = C_{23}$, and $C_{44} = C_{55}$. The six independent elastic constants C_{11}, C_{33}, C_{12}, C_{13}, C_{44}, and C_{66} are calculated as follows. First, since the tetragonal axial ratio c/a generally changes with the volume, by calculating the total energy $E(V, c/a)$ for a series of different c/a ratios at each volume V, we obtain the optimized $(c/a)_0(V)$ from the minimum of $E(V, c/a)$. The volume dependence of $(c/a)_0(V)$ can be related to the difference in the linear compressibilities along the a and c axes. Similarly to the hexagonal case,[53] we introduce a dimensionless quantity R as

$$R = -\frac{d \ln(c/a)_0(V)}{d \ln V}, \quad \text{(A5)}$$

which in terms of tetragonal elastic constants becomes

$$R = \frac{C_{33} - C_{11} - C_{12} + C_{13}}{C_{11} + C_{12} + 2C_{33} - 4C_{13}}. \quad \text{(A6)}$$

Second, at the optimized c/a ratio, the bulk modulus B for a tetragonal crystal can be expressed as

$$B = \frac{C_{33}(C_{11} + C_{12}) - 2C_{13}^2}{C_{11} + C_{12} + 2C_{33} - 4C_{13}}, \quad \text{(A7)}$$

which, when R is close to zero [the volume dependence of $(c/a)_0$ is very small], reduces to $B = \frac{2}{9}(C_{11} + C_{12} + 2C_{13} + C_{33}/2)$. Then, in order to calculate the elastic constants of a tetragonal crystal, we need to make another four independent volume deformations. Here, we choose the two deformations employed for the fcc crystal, i.e., Eq. (A3) corresponding to the energy change in $\Delta E(\delta) = 2VC'\delta^2 + \mathcal{O}(\delta^4)$ and Eq. (A4) corresponding to the energy change in $\Delta E(\delta) = 2VC_{66}\delta^2 + \mathcal{O}(\delta^4)$. For other two deformations, we choose the orthorhombic deformation

$$\begin{pmatrix} 1 & 0 & \delta \\ 0 & \dfrac{1}{1-\delta^2} & 0 \\ \delta & 0 & 1 \end{pmatrix}, \quad \text{(A8)}$$

leading to the energy change in $\Delta E(\delta) = 2VC_{44}\delta^2 + \mathcal{O}(\delta^4)$, and monoclinic deformation

$$\begin{pmatrix} 1+\delta & 0 & 0 \\ 0 & 1 & 0 \\ 0 & 0 & \dfrac{1}{1+\delta} \end{pmatrix}, \quad \text{(A9)}$$

generating the energy change in $\Delta E(\delta) = \frac{1}{2}V(C_{11} - 2C_{13} + C_{33})\delta^2 + \mathcal{O}(\delta^4)$.

The tetragonal phase of In-Tl can be described either as a fct or as a bct structure. In the present work, we calculate the elastic constants in the bct structure. Then the elastic constants for the fct structure are obtained by the following transformations:[54]

$$C_{11}|_{\text{fct}} = \frac{1}{2}(C_{11} + C_{12} + 2C_{66})|_{\text{bct}},$$

$$C_{12}|_{\text{fct}} = \frac{1}{2}(C_{11} + C_{12} - 2C_{66})|_{\text{bct}},$$

$$C_{13}|_{\text{fct}} = C_{13}|_{\text{bct}},$$

$$C_{33}|_{\text{fct}} = C_{33}|_{\text{bct}},$$

$$C_{44}|_{\text{fct}} = C_{44}|_{\text{bct}},$$

$$C_{66}|_{\text{fct}} = \frac{1}{2}(C_{11} - C_{12})|_{\text{bct}}. \quad \text{(A10)}$$

Throughout of the present work, in order to get good fitting coefficients, six strains from $\delta=0$ to $\delta=0.05$ with interval of 0.01 are used to calculate the total energies.

*Corresponding author; cmli@imr.ac.cn

[1] L. Guttman, Trans. Metall. Soc. AIME **188**, 1472 (1950).

[2] J. S. Bowles, C. S. Barrett, and L. Guttman, Trans. Metall. Soc. AIME **188**, 1478 (1950).

[3] M. W. Burkart and T. A. Read, Trans. Metall. Soc. AIME **191**, 1516 (1953).

[4] X.-W. Zhou, J. Li, and M. Wuttig, Phys. Rev. B **44**, 10367 (1991).

[5] D. J. Gunton and G. A. Saunders, Solid State Commun. **14**, 865 (1974).

[6] D. B. Novotny and J. F. Smith, Acta Metall. **13**, 881 (1965).

[7] P. Hohenberg and W. Kohn, Phys. Rev. **136**, B864 (1964).

[8] W. Kohn and L. J. Sham, Phys. Rev. **140**, A1133 (1965).

[9] S. H. Yang, M. J. Mehl, and D. A. Papaconstantopoulos, Phys. Rev. B **57**, R2013 (1998).

[10] E. C. Do, Y.-H. Shin, and B.-J. Lee, CALPHAD: Comput. Coupling Phase Diagrams Thermochem. **32**, 82 (2008).

[11] V. Ramamurthy and S. B. Rajendraprasad, J. Phys. Chem. Solids **47**, 1109 (1986).

[12] D. R. Winder and C. S. Smith, J. Phys. Chem. Solids **4**, 128 (1958).

[13] B. S. Chandrasekhar and J. A. Rayne, Phys. Rev. **124**, 1011 (1961).

[14] O. K. Andersen, O. Jepsen, and G. Krier, in *Lectures on Methods of Electronic Structure Calculations*, edited by V. Kumar, O. K. Andersen, and A. Mookerjee (World Scientific, Singapore, 1994), p. 63.

[15] L. Vitos, H. L. Skriver, B. Johansson, and J. Kollár, Comput. Mater. Sci. **18**, 24 (2000).

[16] L. Vitos, Phys. Rev. B **64**, 014107 (2001).

[17] L. Vitos, I. A. Abrikosov, and B. Johansson, Phys. Rev. Lett. **87**, 156401 (2001).

[18] L. Vitos, *Computational Quantum Mechanics for Materials Engineers: The EMTO Method and Applications* (Springer-Verlag, London, 2007).

[19] P. Soven, Phys. Rev. **156**, 809 (1967).

[20] B. L. Gyorffy, Phys. Rev. B **5**, 2382 (1972).

[21] A. Taga, L. Vitos, B. Johansson, and G. Grimvall, Phys. Rev. B **71**, 014201 (2005).

[22] Z. Nabi, L. Vitos, B. Johansson, and R. Ahuja, Phys. Rev. B **72**, 172102 (2005).

[23] L. Vitos, P. A. Korzhavyi, and B. Johansson, Nature Mater. **2**, 25 (2003).

[24] B. Magyari-Köpe, G. Grimvall, and L. Vitos, Phys. Rev. B **66**, 064210 (2002); **66**, 179902(E) (2002).

[25] B. Magyari-Köpe, L. Vitos, and G. Grimvall, Phys. Rev. B **70**, 052102 (2004).

[26] L. Vitos, P. A. Korzhavyi, and B. Johansson, Phys. Rev. Lett. **88**, 155501 (2002).

[27] L. Huang, L. Vitos, S. K. Kwon, B. Johansson, and R. Ahuja, Phys. Rev. B **73**, 104203 (2006).

[28] O. K. Andersen, C. Arcangeli, R. W. Tank, T. Saha-Dasgupta,

G. Krier, O. Jepsen, and I. Dasgupta, in *Tight-Binding Approach to Computational Materials Science*, edited by P. E. A. Turchi, A. Gonis, and L. Colombo, MRS Symposia Proceedings No. 491 (Materials Research Society, Pittsburgh, 1998), pp. 3–34.

[29] J. Kollár, L. Vitos, and H. L. Skriver, in *Electronic Structure and Physical Properties of Solids: The Uses of the LMTO Method*, edited by H. Dreyssé, Lecture Notes in Physics (Springer-Verlag, Berlin, 2000), p. 85.

[30] R. Armiento and A. E. Mattsson, Phys. Rev. B **66**, 165117 (2002).

[31] J. P. Perdew and A. Zunger, Phys. Rev. B **23**, 5048 (1981).

[32] J. P. Perdew, K. Burke, and M. Ernzerhof, Phys. Rev. Lett. **77**, 3865 (1996).

[33] J. P. Perdew, in *Electronic Structure of Solids '91*, edited by P. Ziesche and H. Eschrig (Akademie Verlag, Berlin, 1991), p. 11.

[34] R. W. Vaughan and H. G. Drickamer, J. Phys. Chem. Solids **26**, 1549 (1965).

[35] A. T. Dinsdale, CALPHAD: Comput. Coupling Phase Diagrams Thermochem. **15**, 317 (1991).

[36] J. S. Olsen, L. Gerward, S. Steenstrup, and E. Johnson, J. Appl. Crystallogr. **27**, 1002 (1994).

[37] N. Lanska, O. Söderberg, A. Sozinov, Y. Ge, K. Ullakko, and V. K. Lindroos, J. Appl. Phys. **95**, 8074 (2004).

[38] S. Banik, R. Ranjan, A. Chakrabarti, S. Bhardwaj, N. P. Lalla, A. M. Awasthi, V. Sathe, D. M. Phase, P. K. Mukhopadhyay, D. Pandey, and S. R. Barman, Phys. Rev. B **75**, 104107 (2007).

[39] C. H. Sonu and T. J. O'Keefe, Mater. Charact. **33**, 311 (1994).

[40] J. T. A. Pollock and H. W. King, J. Mater. Sci. **3**, 372 (1968).

[41] T. F. Smith and T. R. Finlayson, Phys. Rev. B **49**, 12559 (1994).

[42] R. W. Meyerhoff and J. F. Smith, Acta Metall. **11**, 529 (1963).

[43] N. G. Pace and G. A. Saunders, Proc. R. Soc. London, Ser. A **326**, 521 (1972).

[44] X. Ren and K. Otsuka, Mater. Sci. Forum **327-328**, 429 (2000).

[45] X. Ren, K. Otsuka, and T. Suzuki, J. Alloys Compd. **355**, 196 (2003).

[46] K. Otsuka and X. Ren, Prog. Mater. Sci. **50**, 511 (2005).

[47] M. Stipcich, L. Mañosa, A. Planes, M. Morin, J. Zarestky, T. Lograsso, and C. Stassis, Phys. Rev. B **70**, 054115 (2004).

[48] Q. M. Hu, R. Yang, J. M. Lu, L. Wang, B. Johansson, and L. Vitos, Phys. Rev. B **76**, 224201 (2007).

[49] Q. M. Hu, C. M. Li, R. Yang, S. E. Kulkova, D. I. Bazhanov, B. Johansson, and L. Vitos, Phys. Rev. B **79**, 144112 (2009).

[50] D. W. Donovan, G. R. Barsch, R. N. Pangborn, and T. R. Finlayson, Acta Metall. Mater. **42**, 1985 (1994).

[51] M. P. Brassington and G. A. Saunders, Proc. R. Soc. London, Ser. A **387**, 289 (1983).

[52] V. L. Moruzzi, J. F. Janak, and K. Schwarz, Phys. Rev. B **37**, 790 (1988).

[53] G. Steinle-Neumann, L. Stixrude, and R. E. Cohen, Phys. Rev. B **60**, 791 (1999).

[54] F. Jona and P. M. Marcus, Phys. Rev. B **63**, 094113 (2001).